arXiv:1104.5477v2 [astro-ph.EP] 22 Dec 2011

# The Atmospheric Chemistry of GJ 1214b: Photochemistry and Clouds

Eliza Miller-Ricci Kempton

*Department of Astronomy and Astrophysics, University of California, Santa Cruz, CA 95064*

ekempton@ucolick.org

Kevin Zahnle

*NASA Ames Research Center, Moffett Field, CA 94035*

Jonathan J. Fortney

*Department of Astronomy and Astrophysics, University of California, Santa Cruz, CA 95064*

## ABSTRACT

Recent observations of the transiting super-Earth GJ 1214b reveal that its atmosphere may be hydrogen-rich or water-rich in nature, with clouds or hazes potentially affecting its transmission spectrum in the optical and very-near-IR. Here we further examine the possibility that GJ 1214b does indeed possess a hydrogen-dominated atmosphere, which is the hypothesis that is favored by models of the bulk composition of the planet. We study the effects of non-equilibrium chemistry (photochemistry, thermal chemistry, and mixing) on the planet's transmission spectrum. We furthermore examine the possibility that clouds could play a significant role in attenuating GJ 1214b's transmission spectrum at short wavelengths. We find that non-equilibrium chemistry can have a large effect on the overall chemical composition of GJ 1214b's atmosphere, however these changes mostly take place above the height in the atmosphere that is probed by transmission spectroscopy. The effects of non-equilibrium chemistry on GJ 1214b's transmission spectrum are therefore minimal, with the largest effects taking place if the planet's atmosphere has super-solar metallicity and a low rate of vertical mixing. Interestingly, we find that the best fit to the observations of GJ 1214b's atmosphere in transmission occur if the planet's atmosphere is deficient in $CH_4$, and possesses a cloud layer at a pressure of $\sim$200 mbar. This is consistent with a picture of efficient methane photolysis, accompanied by formation of organic

haze that obscures the lower atmosphere of GJ 1214b at optical wavelengths. However, for methane to be absent from GJ 1214b's transmission spectrum, UV photolysis of this molecule must be efficient at pressures of greater than $\sim$ 1 mbar, whereas we find that methane only photolyzes to pressures less than 0.1 mbar, even under the most optimistic assumptions. An alternative explanation of the observations of GJ 1214b is that the atmosphere is water-rich, although this interpretation conflicts with the findings of Croll et al. (2011), who measure a low mean molecular weight for the planet's atmosphere. Additional observations at wavelengths corresponding to mid-IR water and methane features in GJ 1214b's transmission spectrum should break the degeneracy between the two possible cases.

*Subject headings:* planetary systems

## 1. Introduction

The transiting super-Earth GJ 1214b is ideally suited to follow-up observations aimed at characterizing the planet's atmosphere due to the fact that it orbits a relatively bright M-star ($I = 11.52$), producing a deep transit with an observed depth of 1.37% (Berta et al. 2010; Charbonneau et al. 2009). The planet additionally transits quite frequently with its 1.58 day orbital period (a = 0.0143 AU), which further facilitates observational follow-up. Recently, the first observations of GJ 1214b's atmosphere were reported by Bean et al. (2010). These observations, taken with the FORS2 instrument on the VLT reveal a flat transmission spectrum in the near-IR from 780 to 1000 nm.

GJ 1214b has an observed mass and radius of 6.55$\pm$0.98 $M_\oplus$ and 2.68$\pm$0.13 $R_\oplus$ (Charbonneau et al. 2009) respectively, implying a low density (1.88 g/cm$^3$) that requires the planet to possess a significant atmosphere (Nettelmann et al. 2010; Rogers & Seager 2010). Models of the interior of GJ 1214b suggest that the planet either possesses a thick hydrogen atmosphere comprising anywhere between 0.05 and 2.5% of the total mass of the planet, or alternatively that GJ 1214b is a water-rich planet with a thick steam atmosphere. Under the water-rich scenario Rogers & Seager (2010) find that the planet must be at least 60% water by mass to reproduce the planet's observed radius to within its 2-$\sigma$ error bar. Nettelmann et al. (2010) find that a similarly large water-to-rock ratio of greater than 6:1 is needed to reproduce the planet's radius at its best-fit value. However, a bulk planetary composition of such high abundances of water is thought to be improbable from a formation standpoint. Intermediate atmospheres between these two end member cases composed of a combination of water vapor and hydrogen gas are also consistent with the planet's observed mass and radius, and these

would require a smaller fraction of water to reproduce the planet's bulk density. Differentiating between the two proposed classes of atmospheres ($H_2$-rich and $H_2O$-rich) has important implications for understanding the formation history of GJ 1214b and other similar super-Earths. A hydrogen-rich atmosphere for this planet implies that GJ 1214b acquired its atmosphere either by accretion of nebular gasses or from outgassing of significant amounts of hydrogen as the planet cooled and solidified from a magma ocean state, whereas a water-rich planetary (and atmospheric) composition implies that the planet formed from ice-rich material beyond the snow line before migrating in to its current location.

Breaking the degeneracy between the two classes of proposed atmospheres is not possible through refined measurements of GJ 1214b's mass and radius, due to significant degeneracies in the mass-radius relationship for solid exoplanets (Valencia et al. 2006; Fortney et al. 2007; Seager et al. 2007; Sotin et al. 2007). Instead, observations of the planet's atmosphere that constrain its composition are necessary to break the degeneracy between an atmosphere composed of either predominantly hydrogen or water vapor. The most straightforward way to ascertain the composition of GJ 1214b's atmosphere is to observe the planet's atmosphere in transmission, owing to the relationship between the amplitude of spectral features in transmission and the mean molecular weight of the planet's atmosphere (Miller-Ricci et al. 2009). This relationship results from the fact that the depth of transmission spectral features is directly proportional to the atmospheric scale height, which in turn varies inversely with the mean molecular weight. For GJ 1214b, a hydrogen-rich atmosphere should produce spectral features in transmission with amplitudes of 0.1-0.3% relative to light from the host star, whereas the signature of a water vapor atmosphere would only be present at the 0.01% level and would be undetectable with most current instrumentation used for exoplanet characterization (Miller-Ricci & Fortney 2010).

Bean et al. (2010) observe a flat transmission spectrum for GJ 1214b between 780 and 1000 nm, which is consistent with a small scale height, high mean molecular weight atmosphere composed of at least 20% $H_2O$ by volume. An alternative interpretation of the data is that GJ 1214b's atmosphere is hydrogen-dominated, but high-altitude clouds or hazes obscure the deeper regions of the planet's atmosphere where molecular absorption features are predicted to originate in transmission over the wavelength range of the Bean et al. (2010) observations. (Here we define clouds as being formed by equilibrium condensation processes, whereas a haze results from the action of photochemistry.) In the case of the Bean et al. (2010) transmission observations, the cloud layer is required to become optically thick at heights corresponding to pressures of less than 200 mbar, in order to be consistent with the data at the 1-$\sigma$ level. Without a cloud layer, transmission observations would probe even higher pressures at the wavelengths of the Bean et al. (2010) observations, due to the low opacities predicted for this spectral range. Because scattering from cloud or haze particles

should be more efficient at short wavelengths, clouds will have a smaller effect on the transmission spectrum at longer wavelengths in the IR where deep molecular absorption bands should still be present – whereas a water-rich atmosphere would produce a flat spectrum at the $\sim 0.1\%$ level across all wavelengths.

For this reason, additional observations taken at infrared wavelengths could serve to confirm or rule out the hydrogen-rich nature of GJ 1214b's atmosphere. Indeed, Croll et al. (2011) find that GJ 1214b produces a deeper transit in Ks-band ($\sim$2.15 $\mu$m) than in J-band ($\sim$1.25 $\mu$m) at the 3-$\sigma$ level, which is consistent with the predicted signature of a hydrogen-rich atmosphere. However, these results have been difficult to rectify with longer wavelength data at 3.6 and 4.5 $\mu$m from Désert et al. (2011), who also find a flat transmission spectrum that is consistent with the Bean et al. (2010) transit depth. This is an issue that we attempt to address in this paper.

Another possibility that has yet to be explored is that disequilibrium chemistry may play a significant role in determining GJ 1214b's transmission spectrum. Previous modeling efforts have only considered hydrogen-rich compositions of GJ 1214b's atmosphere in thermochemical equilibrium with metallicities between 1 and 50 times solar (Miller-Ricci & Fortney 2010) as a starting point, but this may not be a valid assumption for the actual state of the planet's atmosphere. Non-equilibrium chemistry is known to play a strong role in determining the atmospheric composition for many of the planets and (planet-sized moons) in our solar system and is also responsible for the formation of clouds or hazes in the atmospheres of certain solar system bodies (e.g. $H_2SO_4$ clouds on Venus and hydrocarbon hazes on Titan). Processes that can perturb a planetary atmosphere away from a state of thermochemical equilibrium include photochemistry, dynamical mixing and winds, and are ultimately limited by the finite amount of time required for chemical reactions to proceed. Overall, if the timescale for mixing or photochemical destruction of a species is shorter than the timescale for chemical reactions to return the gas ensemble to its equilibrium state, then non-equilibrium chemistry cannot be ignored.

In this paper we study the effects that non-equilibrium chemistry can have on the overall composition of GJ 1214b's atmosphere, assuming that it is composed of hydrogen-rich gas. We apply a photochemical model, which accounts for UV photolysis of molecules, vertical mixing in the atmosphere, and the finite timescales for chemical reactions to proceed. The result is a suite of non-equilibrium chemical compositions for GJ 1214b's atmosphere, based on a grid of assumptions for the planet's metallicity and eddy mixing rate, and UV irradiation by the host star. For the non-equilibrium chemical compositions that we compute, we determine the transmission spectra that would result. We then compare the resulting non-equilibrium transmission spectra against the currently available data for GJ 1214b. We

also delve further into the question of clouds or hazes in GJ 1214b's atmosphere as a possible explanation for the planet's flat transmission spectrum at near-IR wavelengths. The paper is laid out as follows. In Section 2 we describe our methodology and modeling efforts. In Section 3 we present our modeling results for non-equilibrium chemical abundances and the effects on the transmission spectrum of GJ 1214b, along with constraints on clouds in GJ 1214b's atmosphere. In Section 4 we explore the extent to which our non-equilibrium transmission spectra can reproduce the observations of GJ 1214b in transmission. We conclude with some closing remarks and discussion in Section 5.

## 2. Methodology

Most previous efforts to model the atmospheric structure and spectra of transiting exoplanets have relied on the assumption that the planetary atmosphere resides in a state of thermochemical equilibrium (e.g. Seager et al. 2000; Fortney et al. 2005; Miller-Ricci et al. 2009). This assumption holds if the atmospheric temperature is sufficiently high, the planet exists in an isolated environment, and vigorous atmospheric mixing does not occur. However, most transiting extrasolar planets orbit in exceptionally close proximity to their host stars, and they therefore sit in environments that receive high levels of UV irradiation. To first order, UV photolysis is expected to affect the chemistry of the upper atmosphere of these planets, forcing the atmospheric chemistry away from a state of equilibrium. Vertical mixing and winds can additionally mitigate or exacerbate these effects. Already, observational signatures of non-equilibrium chemistry have been observed for several transiting hot Jupiters (e.g. Swain et al. 2008, 2009a,b; Madhusudhan et al. 2011; Madhusudhan & Seager 2011), and it is becoming increasingly clear that the effects of photochemistry on exoplanet atmospheres cannot be entirely ignored.

A number of authors have recently begun researching the effects of non-equilibrium chemistry on the atmospheres of highly irradiated extrasolar planets. A brief description of this work is as follows. Early work was performed by Liang et al. (2004), who looked at the effects of hydrocarbon chemistry on the atmospheres of close-in giant planets. More recently, Zahnle et al. (2009b) and Zahnle et al. (2009a) applied a photochemical model to look at the effects of sulfur and hydrocarbon chemistry, respectively, on hot Jupiter atmospheres using the same model that we have adopted for this paper. Work by Line et al. (2010) additionally studied the effects of photochemistry specifically on the atmosphere of the close-in extrasolar giant planet HD 189733b. Moses et al. (2011) performed the first study to not only look at atmospheric chemistry but also to predict the observational signatures of disequilibrium processes in the atmospheres of transiting exoplanets by modeling transmission

and emission spectra for HD 209458b and HD 189733b with the abundance profiles from their photochemical modeling. Shabram et al. (2011) additionally looked at the effects of non-equilibrium chemistry on the transmission spectrum of the hot Neptune GJ 436b, using the results from the Zahnle et al. (2009a) photochemical models. In a reverse approach Madhusudhan & Seager (2009), Madhusudhan et al. (2011), and Madhusudhan & Seager (2011) have attempted to back out the chemical abundances of certain key species in hot Jupiter atmospheres, based on the appearance of the planets' transmission and emission spectra without using any assumptions of chemical equilibrium. This backward modeling approach will ultimately allow for detailed fitting of data to simultaneously determine atmospheric structure and abundance profiles for a given exoplanet atmosphere. However, the fitting procedure is currently challenged by the fact that the models are under-constrained by the available data. Backward modeling will become particularly useful in the future once full spectra of exoplanet atmospheres become available. In the meantime, given the minimal quantity of available data for GJ 1214b, we use a forward modeling approach in this paper, similar to the work of Moses et al. (2011), to predict the abundance profiles and spectral signature for this transiting super-Earth.

### 2.1. Photochemical Model

We calculate atmospheric abundances for the transiting super-Earth GJ 1214b that result from non-equilibrium chemical processes (photolysis and vertical mixing) using the photochemistry model developed in Zahnle et al. (2009b) and Zahnle et al. (2009a) for hot Jupiter exoplanets. This model is based on the 1-D photochemical kinetics code initially described in Kasting et al. (1989) and Kasting (1990). While GJ 1214b is not a hot Jupiter, this code is generally applicable to exoplanets with hydrogen-rich atmospheres. Since Zahnle et al. (2009a) the code has been completely re-written in the C programming language. Updates have been made to further generalize the code for calculating the composition of any given exoplanet atmosphere. Specific improvements include functionality for using an arbitrary temperature-pressure profile and increased flexibility in the altitude step size, along with a generalized treatment of UV photolysis. We use the photochemical kinetics code to calculate chemical abundances for 61 atomic and molecular species in GJ 1214b's atmosphere as a function of height (parametrized within the code in terms of atmospheric pressure) by simultaneously solving the equations of continuity and flux. In this study, we solve for 698 chemical reactions including 33 photolysis reactions. The reaction rates and photolysis cross sections employed in this work are listed in Zahnle et al. (2009a, their Tables 2 and 3). Reverse reaction rates are calculated using the method outlined in Visscher & Moses (2011) as outlined below.

For reactions of the form A + B → C + D with forward reaction rate $k_f$, the reverse rate (i.e., the rate for C + D → A + B) is $k_r = k_f \exp(-\Delta G/RT)$, where $\Delta G$, the Gibbs free energy, is obtained from enthalpies and entropies of the of the reactants and products, $\Delta G = H_A + H_B - H_C - H_D - T(S_A + S_B - S_C - S_D)$. Associative reactions of the form A+B → AB, the rate for the reverse reaction (dissociation of AB) is $k_r = k_f (kT/P_\circ) \exp(-\Delta G/RT)$, where $P_\circ = 10^6$ dynes/cm$^2$ is one atmosphere. This must be done in both the low pressure and high pressure limits. Similarly, the associative reverse of a dissociative reaction is given by $k_r = k_f (P_\circ/kT) \exp(-\Delta G/RT)$. For this code we have fit the reverse reaction rates to the standard Arrhenius form $k = AT^b \exp(-T/C)$. This maximizes code flexibility and exploits the thermodynamic limit as an error check. The fits can be quite good, although the asymptotic match to the thermodynamic equilibrium limit is imperfect.

For all of our calculations we employ an underlying temperature-pressure (T-P) profile for GJ 1214b's atmosphere that was presented in Miller-Ricci & Fortney (2010) for solar composition gas in chemical equilibrium and assuming planet-wide redistribution of heat (shown also in Figure 7). The effective temperature and surface gravity for this model are $T_{eff} = 555$ K and $g = 8.95$ m/s respectively. We do not include feedback on the T-P profile based on the changes in atmospheric composition that result from the photochemical modeling.

Due to the fact that the vertical eddy mixing rate and the atmospheric metallicity are unknown for GJ 1214b, we generate a grid of models in both of these parameters. For the eddy diffusion coefficient we calculate models with constant mixing rates of $K_{zz} = 10^6$, $10^7$, and $10^9$ cm$^2$/s. For metallicity, we choose values ranging from solar composition to metal enhanced at 1, 5, and 30 times solar. For all of our calculations we use a stellar zenith angle of $\theta = 30^\circ$. We have done some additional tests with higher values of $\theta$ corresponding to longitudes closer to the terminator, and we have found the effects to be minimal, although a slightly lower level of photodissociation is found.

As a lower boundary condition, we assume that GJ 1214b resides in a state of chemical equilibrium at the base of the atmosphere. Generally speaking, deep in the atmosphere of a planet at sufficiently high temperatures and pressures the chemistry should approach thermal equilibrium. However, this may not be valid if the atmosphere is thin, in which case interactions between the planet's surface and its atmosphere should be taken into account. For GJ 1214b, the minimum mass of its hydrogen envelope corresponds to an atmosphere of at least 450 bars, and the temperature at the base the atmosphere should exceed 1175 K based on calculations of the T-P profile. We calculate equilibrium abundances at the base of the atmosphere using the Gibbs free energy minimization code described in Miller-Ricci et al. (2009), which is in turn based on the method outlined in White et al. (1958). Some of the 61

species considered in the photochemistry code are not included in the equilibrium chemistry code because they are not predicted to be present in any significant quantities in equilibrium. For these molecules, we set their initial abundances at the bottom of the atmosphere to an arbitrary low value of $10^{-40}$. We place our lower boundary for all of our models at a pressure of 1000 bars, where the atmospheric temperature is predicted to be $T \approx 1400$ K from the T-P profile that we employ in this work. We have performed limited tests to determine the sensitivity of our results to the pressure that we choose as the bottom boundary of the atmosphere, and we do not find any strong dependencies for pressures greater than 100 bar. We have additionally assured that our lower boundary lies below the height where CO-$CH_4$ quenching takes place (around 100 bar). Below this height we find that the abundance profiles for the carbon-bearing species follow their equilibrium values. We do not attain quenched abundances for $N_2$ and $NH_3$ even at the 1000 bar lower boundary of our atmosphere, but we show in subsequent sections that this does not have a strong effect on our results.

As an upper boundary condition we set a zero flux lid at 1 $\mu$bar with no flow allowed into or out of the top of the atmosphere. From theoretical calculations, GJ 1214b is thought to be potentially undergoing atmospheric mass loss at a rate of $\sim 9 \times 10^8$ g/s (Charbonneau et al. 2009), however this rate is unconstrained by observations and we therefore choose to ignore the effects of mass loss in our photochemical calculations.

To calculate photolysis rates it is necessary to know the amount of stellar UV flux that is absorbed by the planet's atmosphere. However, the UV spectrum of GJ 1214 has not been measured. Generally, M-stars such as GJ 1214 tend to be relatively more active than early-type stars, with stellar activity decreasing as a function of stellar age. In theory, we can place GJ 1214 on a stellar type vs. age diagram (such as from Selsis et al. 2007) to determine its expected level of UV flux. However, given the large uncertainty in the star's age ($6 \pm^4_3$ Gyr; Charbonneau et al. 2009), the constraints that we can place on its UV flux are essentially meaningless. For this reason, we choose to include UV flux as an additional parameter in our grid of photochemical models. We choose stellar spectra that represent two bounding cases of a low and high UV flux as shown in Figure 1. It is our assumption that the actual UV spectrum for GJ 1214 falls somewhere in between these two extremes. For our low UV case, we employ a stellar model with the same $T_{eff}$ and $g_{surf}$ as GJ 1214, which we calculate by interpolating between bracketing models by Hauschildt et al. (1999). The stellar model does not include sources of UV emission due to stellar activity, so it produces a spectrum that drops off precipitously in the UV following the stellar blackbody, which is almost certainly an underestimate for the actual UV flux from GJ 1214. For our high UV case, we take the observed time-averaged spectrum of the active M4.5V flare star AD Leo from Segura et al. (2005) ($T_{eff} = 3400$ K), which is one of the most active known M-stars. The incident stellar spectrum is then calculated at the orbital distance of GJ 1214b, from 100

to 1000 nm, and this flux is used for calculating photodissociation rates for the 33 photolysis reactions included in the photochemical kinetics code.

### 2.2. Transmission Spectrum Modeling

Using the chemical abundances profiles that we obtain from the photochemical modeling, we calculate transmission spectra using the model outlined in Miller-Ricci et al. (2009) for super-Earth exoplanets. We calculate absorption of stellar light along chords through the planet's upper atmosphere and then integrate to determine the total absorption over the entire projected annulus of the planet's atmosphere in transit. This results in a wavelength-dependent transmission spectrum, which we calculate from 0.3 - 30 $\mu$m. As with the photochemical modeling, we employ the T-P profile from Miller-Ricci & Fortney (2010) for a solar composition atmosphere when calculating the spectra.

To calculate the transmission spectra we include opacities for the major molecular absorbers in the optical and IR including $H_2O$ (Freedman et al. 2008; Partridge & Schwenke 1997), $CH_4$ (Freedman et al. 2008; Karkoschka 1994; Strong et al. 1993), $NH_3$, CO (Freedman et al. 2008, and references therein), and $CO_2$ (Rothman et al. 2005). We additionally include absorption from a number of non-equilibrium carbon-bearing species – HCN (Harris et al. 2008), $C_2H_2$, $C_2H_4$, and $C_2H_6$ (Rothman et al. 2005) – which have significant IR cross sections and are predicted to be present at high abundances in some of our photochemical calculations. We caution that some of the opacity lists, especially those for $C_2H_2$, $C_2H_4$, and $C_2H_6$ along with the short wavelength $CH_4$ data may be incomplete. Atomic species with large opacities in the optical – Na and K – are predicted to be condensed out of the atmosphere of GJ 1214b at the heights probed by transmission spectroscopy and are not included in our calculations. We do however include the effects of Rayleigh scattering in the optical for the most abundant molecules in the atmosphere ($H_2$, He, $H_2O$, $CH_4$, $NH_3$, CO, $CO_2$, and $N_2$). We calculate Rayleigh scattering cross sections for each molecule individually according to

$$\sigma = \frac{8\pi}{3}\left(\frac{2\pi}{\lambda}\right)^4 \alpha^2 \tag{1}$$

where $\alpha$ is the polarizability obtained from the CRC Handbook for each molecule. We do not include the effects of additional scattering into or out of the beam or refraction, which has been found to have a minimal effect (Hubbard et al. 2001).

The end result is a suite of 18 transmission spectra for possible chemical compositions of GJ 1214b's atmosphere. Spectra are calculated for three values of metallicity – 1, 5, and 30 times solar; 3 values of $K_{zz}$ – $10^6$, $10^7$, and $10^9$ cm$^2$/s; and two stellar UV input spectra.

## 3. Results

### 3.1. Photochemistry

Results from running the photochemical kinetics code with our suite of 18 permutations on the model parameters are shown in Figure 2 (major atmospheric constituents) and Figure 3 (carbon-bearing molecules). Depending on the input parameters, the resulting atmospheric abundance profiles can differ dramatically from what is obtained from equilibrium chemistry. This is a result of both photochemistry, which breaks apart molecules in the upper atmosphere, and vertical mixing, which redistributes species throughout the atmosphere. Qualitatively, the effect of eddy mixing is to smooth out chemical gradients in the lower atmosphere, resulting in a more evenly distributed chemical composition. In the upper atmosphere the effects of UV photolysis and molecular diffusion dominate.

Chemically, the main source of differences between the predictions of equilibrium chemistry and our photochemical modeling is that certain reactions occur so slowly that the chemistry will never converge to equilibrium before photolysis and mixing take over. Specifically, photolysis of both ammonia and methane occur readily in the upper atmosphere, but reactions that create these molecules are not favored. The end result is that nitrogen and carbon preferentially form into molecules other than methane and ammonia, resulting in lower abundances of both of these species in the upper atmosphere than what is predicted by equilibrium calculations. Nitrogen tends to combine into the very stable $N_2$ molecule and also forms a smaller amount of HCN. Carbon is redistributed into a wide variety of molecules including CO, $CO_2$, $C_2H_2$ (acetylene), $C_2H_4$ (ethylene), $C_2H_6$ (ethane), and HCN (hydrogen cyanide), resulting in a complex carbon chemistry as shown in Figure 3.

In our models using the quiet M-star as the UV input spectrum (dashed lines in Figures 2 and 3) very little UV photolysis takes place. These results can therefore be interpreted as showing the effects of vertical mixing in the absence of any significant photochemistry. In these models, the atmosphere is generally well-mixed, and abundance profiles for most major constituents are constant with height throughout most of the atmosphere until molecular diffusion takes over at high altitudes. This is in sharp contrast to the predictions of equilibrium chemistry that produce strong gradients in the abundances of several key molecules including CO, $CO_2$, and $NH_3$ (dotted lines in Figures 2 and 3). Our model results produce obvious quenched behavior for several molecules at modest depth including CO, $CO_2$ and HCN. For these molecules, abundance profiles clearly follow their equilibrium values at depth, whereas their abundances are fairly constant above the quench point. All of these molecules also display a gradual transition between the quenched regime and the equilibrium regime, which is a result of atmospheric mixing. In the absence of mixing, the abundance profiles would

transition sharply from equilibrium to their constant quenched abundances at the quench point. CO, $CO_2$, and HCN display fully quenched behavior above 1-10 bar. In contrast, $N_2$ and $NH_3$ display quenched behavior even at the very base of the atmosphere for all of our models, which implies that the actual quench point for these species lies deeper than 1000 bar. For this reason, it is possible that the actual abundances of nitrogen-bearing species in GJ 1214b's atmosphere may differ somewhat from the values we report here.

Without high levels of UV irradiation, methane remains the dominant carbon-bearing species throughout the atmosphere and is present at high abundances ranging from 0.1% for solar metallicity atmospheres to 1% when the metallicity is enhanced to 30 × solar. Ammonia and $N_2$ are expected to be the most abundant nitrogen-bearing molecules with $N_2$ becoming increasingly abundant at higher metallicities. Some additional carbon-bearing species appear at moderate abundances for models with low $K_{zz}$ and high metallicity including HCN and $C_2H_6$. Molecular diffusion allows for heavy molecules to preferentially settle out of the atmosphere at pressures lower than $\sim 100$ $\mu$bar for models with $K_{zz}$ of $10^6$ cm$^2$/s and $\sim 10$ $\mu$bar for models with $K_{zz}$ of $10^7$ cm$^2$/s.

For the highly irradiated models, the upper atmosphere chemistry is further complicated by UV photolysis. In these atmospheres, the chemistry is driven by photolysis of methane and ammonia. Ammonia has an appreciable photolysis cross section throughout the UV, making it unstable in the upper atmosphere (see Figure 4). Methane only has a large UV cross section shortward of 1400 Å, but it experiences significant photolysis from Lyman-$\alpha$ photons at 1216 Å. The heights at which $CH_4$ and $NH_3$ are removed from the atmosphere has a strong dependence on the amount of vertical mixing. At higher values of $K_{zz}$, methane and ammonia are lofted higher into the atmosphere, which results in a replenishing source that counteracts the effects of photolysis. As the models increase in metallicity, both methane and ammonia also mantain higher abundances to higher altitudes. This results from the overall higher abundance of each of these molecules at high Z. Ammonia photodissociates at pressures ranging from 0.1 mbar for high metallicity and high $K_{zz}$, to several mbar for solar metallicity and low $K_{zz}$. Methane is stable to somewhat higher altitudes corresponding to pressures of $\sim$10 $\mu$bar for high metallicity and high $K_{zz}$, to $\sim$100 $\mu$bar for low metallicity and low $K_{zz}$. Despite methane's propensity to remain stable even at fairly high altitudes in GJ 1214b's atmosphere, the combination of methane being converted into other carbon-bearing molecules at altitude along with downward transport produces a complex carbon chemistry throughout the atmosphere. For all of the models with high UV irradiation, CO and $CO_2$ abundances steadily increase as a function of altitude until reaching the region of the atmosphere that is affected by molecular diffusion. HCN, $C_2H_2$, $C_2H_4$, and $C_2H_6$ all demonstrate similar behavior with abundances increasing in the upper atmosphere due to photochemical production before tailing off again at the very top of the atmosphere due to

molecular diffusion and UV photolysis. The abundance gradients for each of these species is highly dependent on metallicity and vertical mixing. At high metallicity, HCN, $C_2H_4$, and $C_2H_6$ achieve modest abundances even at the very base of the atmosphere. Here again the effect of mixing is to smooth out vertical chemical gradients, which results in the non-equilibrium carbon species becoming increasingly well-mixed at higher values of $K_{zz}$.

Aside from methane and ammonia, other molecular species such as $H_2O$, $C_2H_2$, $C_2H_4$, $C_2H_6$, and HCN experience significant UV photolysis in the upper atmosphere in all of our highly irradiated models. As a result, the abundances of these molecules diminish rapidly at high altitude ($P \sim 10^{-6}$ bar), even for our models with high $K_{zz}$. Conversely, for the highly irradiated high $K_{zz}$ models, photochemical *production* of $N_2$, CO, and $CO_2$ leads to increasing abundances of these molecules at altitude given their negligible photolysis cross sections over the wavelength range where UV photons readily penetrate the atmosphere. Atomic species along with the OH radical also become increasingly abundant at high altitude as products of photolysis reactions. At low values of $K_{zz}$, molecular diffusion plays a significant role high in the atmosphere, and in this case heavy molecules are not present at altitude due to gravitational settling. For these low $K_{zz}$ models, the upper atmosphere chemistry is driven by a combination of both molecular diffusion and photolysis.

### 3.2. Transmission Spectroscopy

We take the abundance profiles from our photochemical modeling and use these to produce theoretical transmission spectra for GJ 1214b for each of our 18 models. These results are shown in Figure 5 for the highly irradiated atmosphere and Figure 6 for models using the quiet M-star as the input stellar spectrum. In these figures, all of the spectra have been normalized so as to reproduce the observed transit depth of 1.35% in the MEarth filter bandpass spanning 675 to 1050 nm (Charbonneau et al. 2009).

For the low irradiation models, the spectra that we obtain look virtually identical to the spectra calculated using equilibrium chemistry (gray lines in Figure 6). For these models, photodissociation does not play a strong role in perturbing the atmospheric chemistry. While the overall atmospheric chemistry is expected to be more well-mixed from our calculations than what is obtained from equilibrium chemistry, there is very little effect on the species that produce most of the opacity in our models. Water, methane, ammonia, and to a lesser extent CO and $CO_2$ all have significant opacities between 0.3 and 20 $\mu$m. Of these, the spectral features of water and methane dominate the transmission spectrum, and the abundances of these two species do not differ substantially from their predicted equilibrium values at the height probed by transmission spectroscopy (generally $\sim$ 1 mbar, but can vary between

0.1 and 500 mbar). The CO and $CO_2$ abundance profiles from Figures 2 and 3 do differ dramatically from their equilibrium abundances above ∼100 bar, however this is difficult to discern from looking at the transmission spectra. One reason for this is that the CO and $CO_2$ abundances remain low throughout all of our low-irradiation models with CO and $CO_2$ abundances not exceeding $10^{-4}$ and $10^{-5}$ respectively. Additionally most of the predicted CO spectral features overlap with stronger absoprtion features from $H_2O$ and $CH_4$, which essentially swallow up the spectral signature of what would otherwise be an excellent tracer molecule for the presence of atmospheric mixing and photochemistry. For ammonia, we tend to predict somewhat higher abundances than what is obtained from equilibrium predictions, and this has a small effect in increasing the ammonia absorption in features at 1.5 and 10.5 $\mu$m. However, we note that this result is somewhat dependent on the quenching behavior of ammonia at depth and may not be accurate since our photochemical models to not extend down to the $NH_3/N_2$ quench point. We also tend to see very slightly decreased methane absorption in some of the models, but once again, this is a very small effect and is unlikely to be observable.

Perhaps more surprising is the appearance of the spectra using the high-UV irradiation models (Figure 5). Despite markedly different overall atmospheric chemistry than what is predicted from equilibrium expectations, the effect on the transmission spectra here is also fairly minimal. Methane and ammonia photodissociation lead to slightly weaker spectral features for both of these molecules. Additionally, for models with high levels of $CH_4$ photolysis, HCN contributes significant opacity around 14 $\mu$m, and increased abundances of $CO_2$ also add spectral features at 4.3 and 15 $\mu$m for the high metallicity models. It has been previously pointed out that CO and $CO_2$ abundances increase strongly with metallicity (Zahnle et al. 2009a). We find the same result here, and note that we see increasing absorption from $CO_2$ in the transmission spectra as a function of metallicity. Generally, the abundance of $CO_2$ needs to exceed 1 part in $10^5$ for this molecule to be apparent in the transmission spectrum of GJ 1214b. Overall, while the changes in the transmission spectra relative to equilibrium expectations are noticeable, they are not dramatic. The largest effects are seen at low $K_{zz}$ and high metallicity. Given the current quality of observational transmission data, it is likely that it will be difficult to distinguish between the different possibilities with observations. We explore this question further in Section 4

As a note of caution, it is important to point out that transmission spectroscopy specifically probes the region of the atmosphere at the planet's day-night terminator (around the 1 mbar pressure level), since this is where all absorption of stellar light will take place. It is possible that the terminator chemistry is more complex than what we have modeled here for a number of reasons. Since GJ 1214b is expected to be tidally locked to its host star, it is likely that chemical gradients exist between the day and night side of the planet.

Observations of the planet in transmission may therefore be sensitive to the presence of longitudinal winds that carry material from the day side to the night side of the planet, or vice versa. These winds could be an additional contributor to non-equilibrium chemistry that we are unable to address here using our 1-D model (e.g. Cooper & Showman 2006). 3-D models of atmospheric dynamics on hot Jupiters show that strong winds that advect heat from the day side to the night side of the planet should be present at the heights probed by transmission spectroscopy at both the eastern and western terminators (Showman et al. 2008; Dobbs-Dixon et al. 2010; Rauscher & Menou 2010). In this case the chemistry at the terminator should resemble that of the planet's day side, and our use of a day-side chemistry model is justified in calculating transmission spectra for GJ 1214b (e.g. Fortney et al. 2010). However, we caution that it is unclear how to scale the dynamical models for hot Jupiters to a super-Earth like GJ 1214b, and therefore the atmospheric circulation for this planet is unconstrained at this point in time.

### 3.3. Clouds and Hazes

Clouds would further complicate the appearance of the planet's transmission spectrum by efficiently scattering starlight at short wavelengths. At longer wavelengths in the mid-IR, the spectrum of GJ 1214b should remain mostly unaffected by clouds. Qualitatively, in the optical and near-IR, clouds can flatten the planet's transmission spectrum by scattering light at higher altitudes than where spectral features in transmission are expected to originate. For GJ 1214b, we have previously found that clouds at pressures greater than 200 mbar can explain the observations of a flat transmission spectrum from 780 to 1000 nm by Bean et al. (2010). This value was determined by cutting off transmission at different heights in the planet's atmosphere to simulate the effects of an optically thick gray cloud deck. Clouds deeper in the atmosphere than 200 mbar would have only a minimal effect on the transmission spectrum at the wavelengths of the Bean et al. (2010) observations. If clouds are present, the exact shape of the transmission spectrum at short wavelengths is determined by whether the scattering is occurring within the Rayleigh or Mie regime, which will produce different power law slopes for the scattering opacity. Unfortunately, self-consistently modeling the cloud opacity requires knowledge of the cloud particle size and height distributions, which are currently unknown for GJ 1214b. Here we offer up some suggestions for what the cloud composition could be.

Clouds are formed by condensation processes, which will occur if the partial pressure of a species surpasses its vapor or condensation pressure. To determine whether cloud formation will occur in the atmosphere of GJ 1214b, we compare the planet's T-P profile against the

condensation curves of various molecules that are predicted to condense in hot planet and cool star atmospheres from Lodders & Fegley (2006). The only molecules that we find whose condensation curves intersect the predicted T-P profile of GJ 1214b are KCl and ZnS, as shown in Figure 7, although we caution that the T-P profile of GJ 1214b is unconstrained by observations, so its exact shape is somewhat uncertain. If the T-P profile from Figure 7 is correct, then both KCl and ZnS should condense at pressures of ∼500 mbar in GJ 1214b's atmosphere at solar composition. For higher metallicities a number of effects come into play which can shift the condensation to either higher or lower pressure in GJ 1214b's atmosphere. These effects are (1) the abundaces of condensate materials tend to be higher at higher Z, (2) the condensation curves for condensate species tend to shift to higher temperature i.e. to the right on Figure 7 due to the increased vapor pressure of the heavy elements in the gas phase, and (3) the T-P profile tends to shift up and to right on Figure 7 due to the increased opacities from higher metal abundances at high metalicity. The first two of these effects will push condensation to higher pressures where a deeper and more massive cloud layer will form. The third effect (shifting the T-P profile) will have the opposite effect of pushing condensation to higher in the atmosphere at lower pressure. KCl and ZnS are both predicted to be present at very low abundances under the assumption of equilibrium, so it is unclear if either of these species could be present in large enough quantities to form an optically thick cloud. The predicted equilibrium abundance for KCl at 500 mbar and 800 K is only $8.5 \times 10^{-9}$ at solar metallicity and $1.5 \times 10^{-6}$ at 30 × solar metallicity. We do not calculate abundances for ZnS in our equilibrium chemistry code since we only include the 22 most abundant atomic elements from the Sun. Zinc's abundance in the Sun is only $1.5 \times 10^{-8}$ (Asplund et al. 2005), and ZnS is likely to be present in even lower amounts in GJ 1214b's atmosphere. However, due to the fact that GJ 1214b is viewed in transmission along a slant optical path, even low abundances of condensate particles can form an optically thick cloud. Fortney (2005) explored this issue and found that condensed KCl may form a cloud with an optical depth of ∼0.18 in a solar composition hot Jupiter atmosphere, whereas ZnS should only form a cloud of optical depth ∼0.09.

Another possibility is that GJ 1214b may form photochemical hazes in its atmosphere. The composition of any such hazes is unconstrained due to the complex nature of the photochemical processes that would lead to their formation. However, we can look to solar system objects to inform our understanding of possible haze formation mechanisms for GJ 1214b. Photochemically induced hazes are common in the atmospheres of solar system planets and planet-sized moons. Among the nearby planets, Venus possesses a sulfuric acid haze layer in its atmosphere. Additionally, a number of solar system objects including Jupiter, Neptune, and Titan have hazes composed of complex hydrocarbons. Hazes may be common in exoplanet atmospheres as well. The transiting hot Jupiter HD 189733b has an optical trans-

mission spectrum that is consistent with a high altitude haze (Sing et al. 2011; Pont et al. 2008), although its composition is currently unconstrained. Of the solar system haze scenarios, it is most likely that GJ 1214b forms hydrocarbon hazes in its atmosphere, given the high abundance of methane that we predict. Many of our photochemical models from Section 3.1 produce large amounts of the second-order hydrocarbons $C_2H_2$, $C_2H_4$, and $C_2H_6$, which are the first byproducts in the sequence of chemical reactions to form the high-level hydrocarbons that would make up a Titan-like haze. Unsaturated hydrocarbons such as $C_2H_2$ have a propensity to polymerize, eventually forming complex molecules such as PAH's, tholins, and soots (e.g. Yung et al. 1984). Unfortunately, our photochemical code does not include reactions for hydrocarbons of higher order than $C_2H_X$, so we cannot predict the exact composition or abundance profiles for the haze layer. We can however state that GJ 1214b should be amenable to forming hydrocarbon haze in its atmosphere.

## 4. Confronting the Observations

A number of observational studies of GJ 1214b's atmosphere have already taken place, and here we attempt to rectify our modeling efforts with the available data. To date, observations of GJ 1214b's atmosphere have been focused on transit measurements to determine the planet's effective radius as a function of wavelength (transmission spectrum). An alternative observing strategy would be to observe GJ 1214b at secondary eclipse to obtain day-side emission spectroscopy. Unfortunately, the expected secondary eclipse depth for GJ 1214b at wavelengths shortward of 5 $\mu$m is less than 100 ppm (Miller-Ricci & Fortney 2010) and is therefore likely to remain beyond the reach of observational detection for current instrumentation. In the meantime, transmission spectroscopy has the added benefit of being highly sensitive to the atmospheric mean molecular weight, which allows for a better understanding of the bulk composition of the atmosphere.

The observational efforts to date are summarized as follows. The MEarth survey produced the original measurement of GJ 1214b's transit depth using a broad-band optical/near-IR filter spanning ∼675-1050 nm (Charbonneau et al. 2009). These transit observations produced a transit depth of 1.35%, which was later refined by Berta et al. (2010) to 1.37% using additional epochs of MEarth observations along with transit observations from the VLT and FLWO 1.2-meter telescope. Kundurthy et al. (2010) further extended the transit observations to shorter wavelengths at $r$-band, obtaining a transit depth of $(R_p/R_\star)^2 = 0.01084 \pm 0.00056$. However, their $r$-band data is highly degenerate with limb darkening, and including the formal error bars on their limb darkening parameters leads to a much larger error bar in the transit depth. Bean et al. (2010) produced the first wavelength-dependent

transmission spectrum in the very-near-IR from 780 to 1000 nm, using the FORS2 instrument on the VLT. The resulting transmission spectrum is featureless, as discussed in Section 1. Désert et al. (2011) provide two additional data points to the transmission spectrum at longer wavelengths in the IR using the two warm Spitzer IRAC channels. Their 3.6 and 4.5 $\mu$m data continue to reveal a flat transmission spectrum at high significance. Croll et al. (2011) are the only authors to report a wavelength dependent *variation* in transit depth for GJ 1214b. Their J and Ks band data show a strong discrepancy between the transit depths observed at these two wavelengths at a level of several sigma. This is attributed to GJ 1214b having a hydrogen-rich atmosphere with a large scale height, which is the only way to produce such a large difference between the transit depths observed at two separate wavelengths.

Here we attempt to fit all the available data with our modeled transmission spectra from Section 2.2. We compare each of our modeled spectra to the observed transit depths from all of the data sets where multi-wavelength data was obtained, and we compute a goodness-of-fit ($\chi^2$) parameter to assess how well each model reproduces the data. We perform a comparison to the ensemble of multi-wavelength data from Bean et al. (2010), Désert et al. (2011), and Croll et al. (2011). We additionally do a comparison between our models and only the combined Désert et al. (2011), and Croll et al. (2011) data, under the assumption that the Bean et al. (2010) data at wavelengths shortward of 1 $\mu$m are affected by the presence of clouds. We normalize all of our models vertically such that the best fit to the data is achieved, and we do not allow for vertical offsets between the individual datasets, which would introduce an unnecessarily large number of free parameters into our analysis. While GJ 1214 is known to be an active and spotted star, the wavelength-dependent effect on the transit depth should be minimal and has already been accounted for in the observational studies.

We compare the data against a total of 27 different transmission spectrum models that we have generated (listed in Table 1). The first 18 are the results of our photochemical modeling, shown in Figures 5 and 6. Four of the remaining models are for hydrogen-rich atmospheres – three are equilibrium compositions of 1, 30, and 50 times solar metallicity from Miller-Ricci & Fortney (2010), and the fourth is a solar composition (equilibrium) atmosphere with methane artificially removed simulating the effect of much stronger UV photolysis than what we have reported in Section 3.1. The remaining five models are for atmospheres with increasing mean molecular weight due to higher abundances of water relative to $H_2$. We calculate models consisting of 10, 20, 30, 40, and 100% $H_2O$, with the remaining portion of the atmosphere composed of $H_2$.

For the combination of all of the available spectral data from Bean et al. (2010), Désert et al.

(2011), and Croll et al. (2011), the best fit is achieved for an atmosphere composed of 100% water vapor. The quality of the fit is not very good, remaining consistent with the ensemble of data at only the 2-$\sigma$ level. Here the fit to the model is dominated by the 11 data points from Bean et al. (2010), which are an excellent match to the flat spectrum produced by a high mean molecular weight water atmosphere. However, the Croll et al. (2011) Ks-band data point remains highly inconsistent with the steam atmosphere model at more than 5-$\sigma$ (see Figure 8). It is tempting to consider the Croll et al. (2011) Ks-band point as a statistical outlier under the steam atmosphere scenario. However, we point out that the Croll et al. (2011) results are robust in that three separate transits were observed in their study, and during all three events the Ks band transit was observed to be deeper than the J-band transit by a comparable magnitude.

Given the poor model fits to the combination of all of the available transmission data, we consider the possibility that the Bean et al. (2010) results are influenced by clouds, but that the longer wavelength data remain unaffected. Fitting the Désert et al. (2011) and Croll et al. (2011) data alone, we find that the best fit is achieved for a solar composition atmosphere with methane artificially removed. The quality of the fit is quite good and is consistent with the data at 1-$\sigma$. The no-methane interpretation is intriguing in that it requires methane to be absent from the atmosphere at pressures of $\sim$1 mbar, where the transmission spectrum originates. This directly contradicts the results of our photochemical modeling from Section 3.1 where we found that methane should only photolyze to pressures of less than $\sim$0.1 mbar and below this height it should be quite abundant. One possibility to rectify this discrepancy is that GJ 1214b's atmosphere has an eddy diffusion rate of less than $10^6$ at altitude, which would allow for methane to be removed from the atmosphere at lower altitudes and higher pressures. Another possibility is that we have underestimated the UV flux incident on the planet's upper atmosphere, although this is unlikely given that AD Leo is one of the most active known M-stars, and we used its UV spectrum for our high-irradiation models.

The no-$CH_4$ model provides a poor fit to all of the available data when the Bean et al. (2010) data is added in. However, if we assume that clouds affect the short-wavelength data, then this is to be expected. To simulate the effect of clouds in the wavelength range of the Bean et al. (2010) data, we increase the amount of Rayleigh scattering by a factor of 5, which raises the height at which the atmosphere becomes optically thick from scattering. We find that this provides a much improved fit to the data (see Figure 8). The no-$CH_4$ atmosphere with increased Rayleigh scattering is consistent with the combination of the Bean et al. (2010), Désert et al. (2011), and Croll et al. (2011) at a level of 1.5-$\sigma$. The Bean et al. (2010) data alone similarly gives a 1.5-$\sigma$ fit to the no-$CH_4$ increased Rayleigh scattering model. Even with the increased Rayleigh scattering, a water feature is expected

to be present in the transmission spectrum at 970 nm, which is absent from the Bean et al. (2010) data, but the discrepancy here is still less than only 2-$\sigma$.

If clouds are indeed the explanation for the short wavelength transmission data, the exact form of cloud scattering would differ from a simple $\lambda^{-4}$ power law for Rayleigh scattering. Scattering occurs in the Rayleigh regime only if the particle size in the cloud layer is much smaller than the wavelength of the light. For larger particle sizes approaching 1 $\mu$m Mie scattering is expected, which should produce a shallower slope, more closely approximating a gray cloud deck. However, comparisons to forms of cloud opacity other than those approximated by Rayleigh scattering are beyond the scope of this work. Observations that extend to shorter wavelengths and also filling in the data gap between 1 and 1.5 $\mu$m should help to further constrain the power law slope on the scattering opacity which could in turn provide hints as to the composition of the cloud deck.

## 5. Conclusions and Discussion

While photochemistry should play an important role in determining the atmospheric chemistry of GJ 1214b, we find that its effects are minimal at the heights probed by transmission spectroscopy. We find only minor differences between our modeled transmission spectra for equilibrium chemistry and the spectra resulting from our more detailed photochemical modeling. Methane and ammonia photolysis are expected to alter the atmospheric chemistry by allowing additional carbon- and nitrogen-bearing molecules to form, some of which do not appear in significant abundances under the assumption of chemical equilibrium. However, the effects of non-equilibrium chemistry do not extend to pressures greater than 1 mbar at a sufficient level to have any major effects on our modeled transmission spectra.

When fitting the available transmission spectroscopy data for GJ 1214b however, an intriguing possibility is raised that methane photolysis may be much more efficient than what we predict from our photochemical modeling. The transmission data are best fit by a model with no methane and clouds or hazes that affect the optical and near-IR spectrum. This is consistent with GJ 1214b having a hydrogen-rich atmosphere where methane is efficiently photolyzed, and carbon-rich hazes form readily.

Still, much degeneracy remains in the modeling efforts, which is due partly to the small amount of spectral data available for GJ 1214b's atmosphere. Additional data will provide much-needed constraints to our modeling efforts. It still remains to be confirmed that GJ 1214b does indeed possess a low mean molecular weight atmosphere. This interpretation is so far based upon a single Ks-band data point from Croll et al. (2011), which should

be corroborated with additional data. If methane is absent from GJ 1214b's atmosphere, then confirmation of GJ 1214b's low mean molecular weight through the observation of deep spectral features in transmission should be done by observing water features in the planet's spectrum at wavelengths longward of 1-2 $\mu$m where the effects of clouds should not be significant. Additional observations at the wavelengths of methane features are also needed to confirm that this molecule is truly absent from the transmission spectrum. The interpretation of a low methane abundance so far depends strongly on the flat transmission spectrum observed by Désert et al. (2011) with warm Spitzer, who should have seen strong methane absorption in the 3.6 $\mu$m IRAC band if this molecule was present in modest abundances.

If GJ 1214b's atmosphere does in fact have a high mean molecular weight, then the atmosphere must be water-rich to be consistent with models of the interior of the planet (e.g. Rogers & Seager 2010). In this case the photochemistry should be driven by photolysis of water into OH and H. Such an atmosphere would surely be affected by escape of atomic hydrogen, resulting in the atmosphere slowly becoming more oxidized with time. The level of oxidation of the atmosphere should then be highly dependent on the rate of atmospheric escape, which is currently unconstrained. Additional study of the photochemistry of a water-rich atmosphere for GJ 1214b is beyond the scope of this work but merits additional investigation.

GJ 1214b is now one of a growing group of transiting super-Earth exoplanets. To date, 8 transiting super-Earths have been confirmed, and another 288 "super-Earth" candidates from Kepler with radii between 1.25 and 2 $R_\oplus$ still await confirmation (Borucki et al. 2011). Additionally, some of the 662 "Neptune-like" Kepler candidates with radii between 2 and 6 $R_\oplus$ may also fit into the super-Earth category, when defined as in this paper by planets with masses between 1 and 10 $M_\oplus$. Interestingly, GJ 1214b falls into the latter category of planets that would be defined as "Neptune-class" by the Kepler standards. Looking at the current population of 8 transiting super-Earths, there seems to be a wide range of implied bulk composition of these planets, ranging from the iron-rich planet Kepler-10b (Batalha et al. 2011) to the hydrogen-rich planet Kepler-11e (Lissauer et al. 2011). GJ 1214b fits in somewhere in the middle of this population of planets, with its middle-of-the-road density of 1.9 g/cm$^3$ and implied composition that is either ice-rich or hydrogen-rich (or somewhere in between these two extremes). Ultimately, a combination of mass and radius measurements along with atmospheric studies such as the one presented here will allow for stronger constraints to be placed on the bulk composition of these planets, which will in turn give us a more detailed understanding of the formation and evolution processes that give rise to the observed population of super-Earths.

E. M.-R. K was supported by a contract with the California Institute of Technology

funded by NASA through the Sagan Fellowship Program.

## REFERENCES

Asplund, M., Grevesse, N., & Sauval, A. J. 2005, in Astronomical Society of the Pacific Conference Series, Vol. 336, Cosmic Abundances as Records of Stellar Evolution and Nucleosynthes is, ed. T. G. Barnes, III & F. N. Bash, 25–+

Batalha, N. M., et al. 2011, ApJ, 729, 27

Bean, J. L., Kempton, E., & Homeier, D. 2010, Nature, 468, 669

Berta, Z. K., Charbonneau, D., Bean, J., Irwin, J., Burke, C. J., Désert, J., Nutzman, P., & Falco, E. E. 2010, ArXiv e-prints

Borucki, W. J., et al. 2011, ArXiv e-prints

Charbonneau, D., et al. 2009, Nature, 462, 891

Cooper, C. S., & Showman, A. P. 2006, ApJ, 649, 1048

Croll, B., Albert, L., Jayawardhana, R., Miller-Ricci Kempton, E., Fortney, J. J., Murray, N., & Neilson, H. 2011, ArXiv e-prints

Désert, J., et al. 2011, ArXiv e-prints

Dobbs-Dixon, I., Cumming, A., & Lin, D. N. C. 2010, ApJ, 710, 1395

Fortney, J. J. 2005, MNRAS, 364, 649

Fortney, J. J., Marley, M. S., & Barnes, J. W. 2007, ApJ, 659, 1661

Fortney, J. J., Marley, M. S., Lodders, K., Saumon, D., & Freedman, R. 2005, ApJ, 627, L69

Fortney, J. J., Shabram, M., Showman, A. P., Lian, Y., Freedman, R. S., Marley, M. S., & Lewis, N. K. 2010, ApJ, 709, 1396

Freedman, R. S., Marley, M. S., & Lodders, K. 2008, ApJS, 174, 504

Harris, G. J., Larner, F. C., Tennyson, J., Kaminsky, B. M., Pavlenko, Y. V., & Jones, H. R. A. 2008, MNRAS, 390, 143

Hauschildt, P. H., Allard, F., & Baron, E. 1999, ApJ, 512, 377

Hubbard, W. B., Fortney, J. J., Lunine, J. I., Burrows, A., Sudarsky, D., & Pinto, P. 2001, ApJ, 560, 413

Karkoschka, E. 1994, Icarus, 111, 174

Kasting, J. F. 1990, Origins of Life and Evolution of the Biosphere, 20, 199

Kasting, J. F., Zahnle, K. J., Pinto, J. P., & Young, A. T. 1989, Origins of Life and Evolution of the Biosphere, 19, 95

Kundurthy, P., Agol, E., Becker, A. C., Barnes, R., Williams, B., & Mukadam, A. 2010, ArXiv e-prints

Liang, M., Seager, S., Parkinson, C. D., Lee, A., & Yung, Y. L. 2004, ApJ, 605, L61

Line, M. R., Liang, M. C., & Yung, Y. L. 2010, ApJ, 717, 496

Lissauer, J. J., et al. 2011, Nature, 470, 53

Lodders, K., & Fegley, Jr., B. 2006, Chemistry of Low Mass Substellar Objects, ed. Mason, J. W. (Springer Verlag), 1–+

Madhusudhan, N., et al. 2011, Nature, 469, 64

Madhusudhan, N., & Seager, S. 2009, ApJ, 707, 24

—. 2011, ApJ, 729, 41

Miller-Ricci, E., & Fortney, J. J. 2010, ApJ, 716, L74

Miller-Ricci, E., Seager, S., & Sasselov, D. 2009, ApJ, 690, 1056

Moses, J. I., et al. 2011, ArXiv e-prints

Nettelmann, N., Fortney, J. J., Kramm, U., & Redmer, R. 2010, ArXiv e-prints

Partridge, H., & Schwenke, D. W. 1997, J. Chem. Phys., 106, 4618

Pont, F., Knutson, H., Gilliland, R. L., Moutou, C., & Charbonneau, D. 2008, MNRAS, 385, 109

Rauscher, E., & Menou, K. 2010, ApJ, 714, 1334

Rogers, L. A., & Seager, S. 2010, ApJ, 716, 1208

Rothman, L. S., et al. 2005, Journal of Quantitative Spectroscopy and Radiative Transfer, 96, 139

Seager, S., Kuchner, M., Hier-Majumder, C., & Militze r, B. 2007, ArXiv e-prints, 707

Seager, S., Whitney, B. A., & Sasselov, D. D. 2000, ApJ, 540, 504

Segura, A., Kasting, J. F., Meadows, V., Cohen, M., Scalo, J., Crisp, D., Butler, R. A. H., & Tinetti, G. 2005, Astrobiology, 5, 706

Selsis, F., Kasting, J. F., Levrard, B., Paillet, J., Ribas, I., & Delfosse, X. 2007, A&A, 476, 1373

Shabram, M., Fortney, J. J., Greene, T. P., & Freedman, R. S. 2011, ApJ, 727, 65

Showman, A. P., Cooper, C. S., Fortney, J. J., & Marley, M. S. 2008, ApJ, 682, 559

Sing, D. K., et al. 2011, ArXiv e-prints

Sotin, C., Grasset, O., & Mocquet, A. 2007, Icarus, 191, 337

Strong, K., Taylor, F. W., Calcutt, S. B., Remedios, J. J., & Ballard, J. 1993, Journal of Quantitative Spectroscopy and Radiative Transfer, 50, 363

Swain, M. R., et al. 2009a, ApJ, 704, 1616

Swain, M. R., Vasisht, G., & Tinetti, G. 2008, Nature, 452, 329

Swain, M. R., Vasisht, G., Tinetti, G., Bouwman, J., Chen, P., Yung, Y., Deming, D., & Deroo, P. 2009b, ApJ, 690, L114

Valencia, D., O'Connell, R. J., & Sasselov, D. 2006, Icarus, 181, 545

Visscher, C., & Moses, J. I. 2011, ArXiv e-prints

White, W. B., Johnson, S. M., & Dantzig, G. B. 1958, J. Chem. Phys., 28, 751

Yung, Y. L., Allen, M., & Pinto, J. P. 1984, ApJS, 55, 465

Zahnle, K., Marley, M. S., & Fortney, J. J. 2009a, ArXiv e-prints

Zahnle, K., Marley, M. S., Freedman, R. S., Lodders, K., & Fortney, J. J. 2009b, ApJ, 701, L20

This preprint was prepared with the AAS LaTeX macros v5.2.

Table 1. Transmission Spectra Models

| | |
|---|---|
| 1 | Solar Composition |
| 2 | 30 × Solar Composition |
| 3 | 50 × Solar Composition |
| 4 | Solar Composition w/ no $CH_4$ |
| 5 | 10% $H_2O$, 90% $H_2$ |
| 6 | 20% $H_2O$, 80% $H_2$ |
| 7 | 30% $H_2O$, 70% $H_2$ |
| 8 | 40% $H_2O$, 60% $H_2$ |
| 9 | 100% $H_2O$ (steam) |
| 10 | Photochemistry – 1 × Solar, $K_{zz} = 10^9$ cm$^2$/s, Quiet M-star |
| 11 | Photochemistry – 1 × Solar, $K_{zz} = 10^7$ cm$^2$/s, Quiet M-star |
| 12 | Photochemistry – 1 × Solar, $K_{zz} = 10^6$ cm$^2$/s, Quiet M-star |
| 13 | Photochemistry – 5 × Solar, $K_{zz} = 10^9$ cm$^2$/s, Quiet M-star |
| 14 | Photochemistry – 5 × Solar, $K_{zz} = 10^7$ cm$^2$/s, Quiet M-star |
| 15 | Photochemistry – 5 × Solar, $K_{zz} = 10^6$ cm$^2$/s, Quiet M-star |
| 16 | Photochemistry – 30 × Solar, $K_{zz} = 10^9$ cm$^2$/s, Quiet M-star |
| 17 | Photochemistry – 30 × Solar, $K_{zz} = 10^7$ cm$^2$/s, Quiet M-star |
| 18 | Photochemistry – 30 × Solar, $K_{zz} = 10^6$ cm$^2$/s, Quiet M-star |
| 19 | Photochemistry – 1 × Solar, $K_{zz} = 10^9$ cm$^2$/s, AD Leo (Active Star) |
| 20 | Photochemistry – 1 × Solar, $K_{zz} = 10^7$ cm$^2$/s, AD Leo (Active Star) |
| 21 | Photochemistry – 1 × Solar, $K_{zz} = 10^6$ cm$^2$/s, AD Leo (Active Star) |
| 22 | Photochemistry – 5 × Solar, $K_{zz} = 10^9$ cm$^2$/s, AD Leo (Active Star) |
| 23 | Photochemistry – 5 × Solar, $K_{zz} = 10^7$ cm$^2$/s, AD Leo (Active Star) |
| 24 | Photochemistry – 5 × Solar, $K_{zz} = 10^6$ cm$^2$/s, AD Leo (Active Star) |
| 25 | Photochemistry – 30 × Solar, $K_{zz} = 10^9$ cm$^2$/s, AD Leo (Active Star) |
| 26 | Photochemistry – 30 × Solar, $K_{zz} = 10^7$ cm$^2$/s, AD Leo (Active Star) |
| 27 | Photochemistry – 30 × Solar, $K_{zz} = 10^6$ cm$^2$/s, AD Leo (Active Star) |

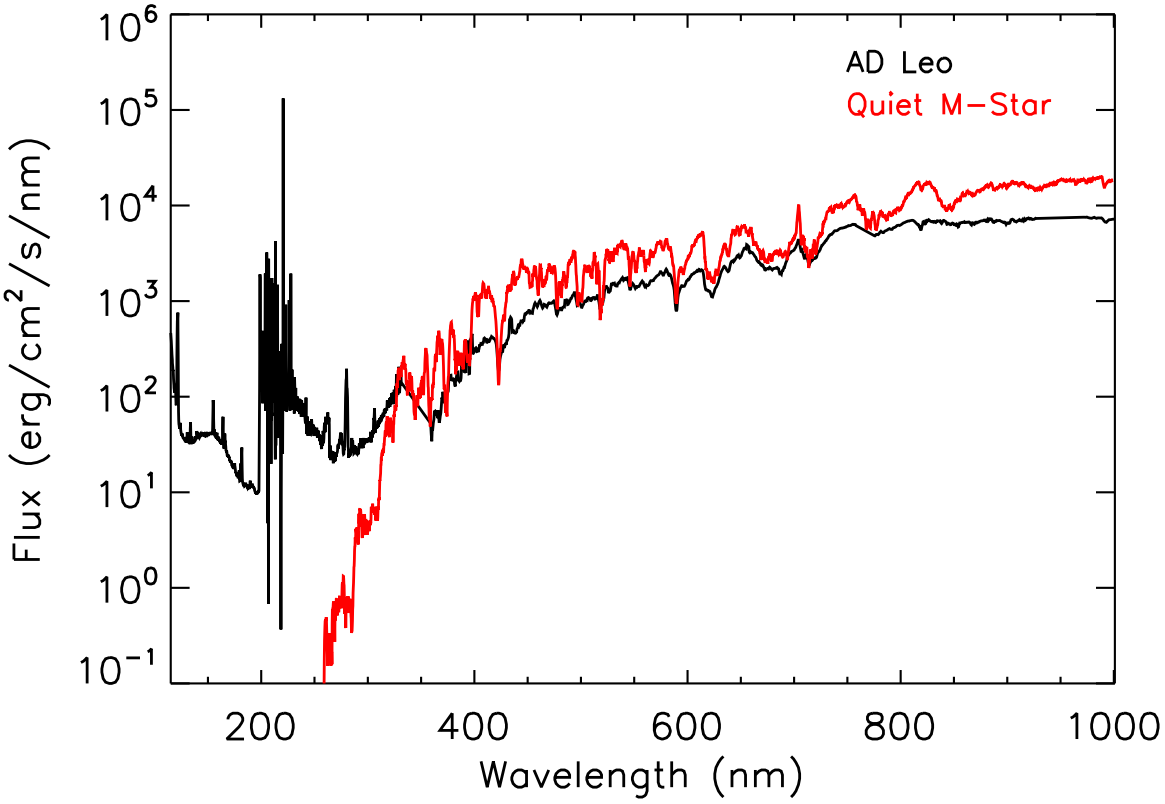


Fig. 1.— Spectra for the two stars that we use in our photochemical modeling. The red line is a modeled spectrum for a quiet M-star from Hauschildt et al. (1999). The black line is the time-averaged spectrum of the M4.5V star AD Leo from Segura et al. (2005). The fluxes listed on the y-axis are the incident fluxes at the orbital distance of GJ 1214b (a = 0.0143 AU).

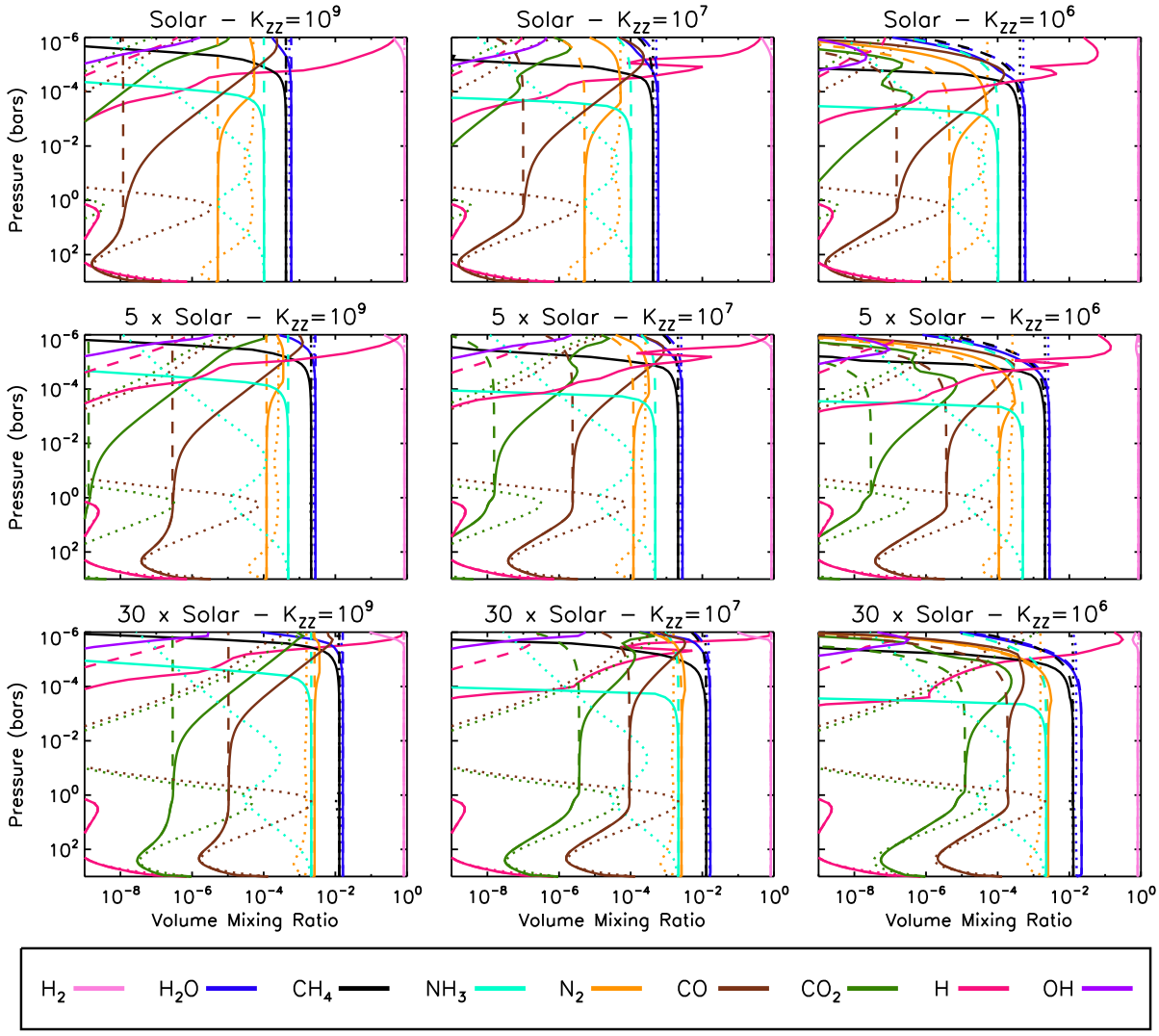


Fig. 2.— Results from our photochemical calculations for the major atmospheric constituents. Models using the quiet M-star as the stellar input spectrum are shown with dashed lines. Models using AD Leo as the input spectrum are shown with solid lines. Equilibrium abundances are shown with dotted lines for reference.

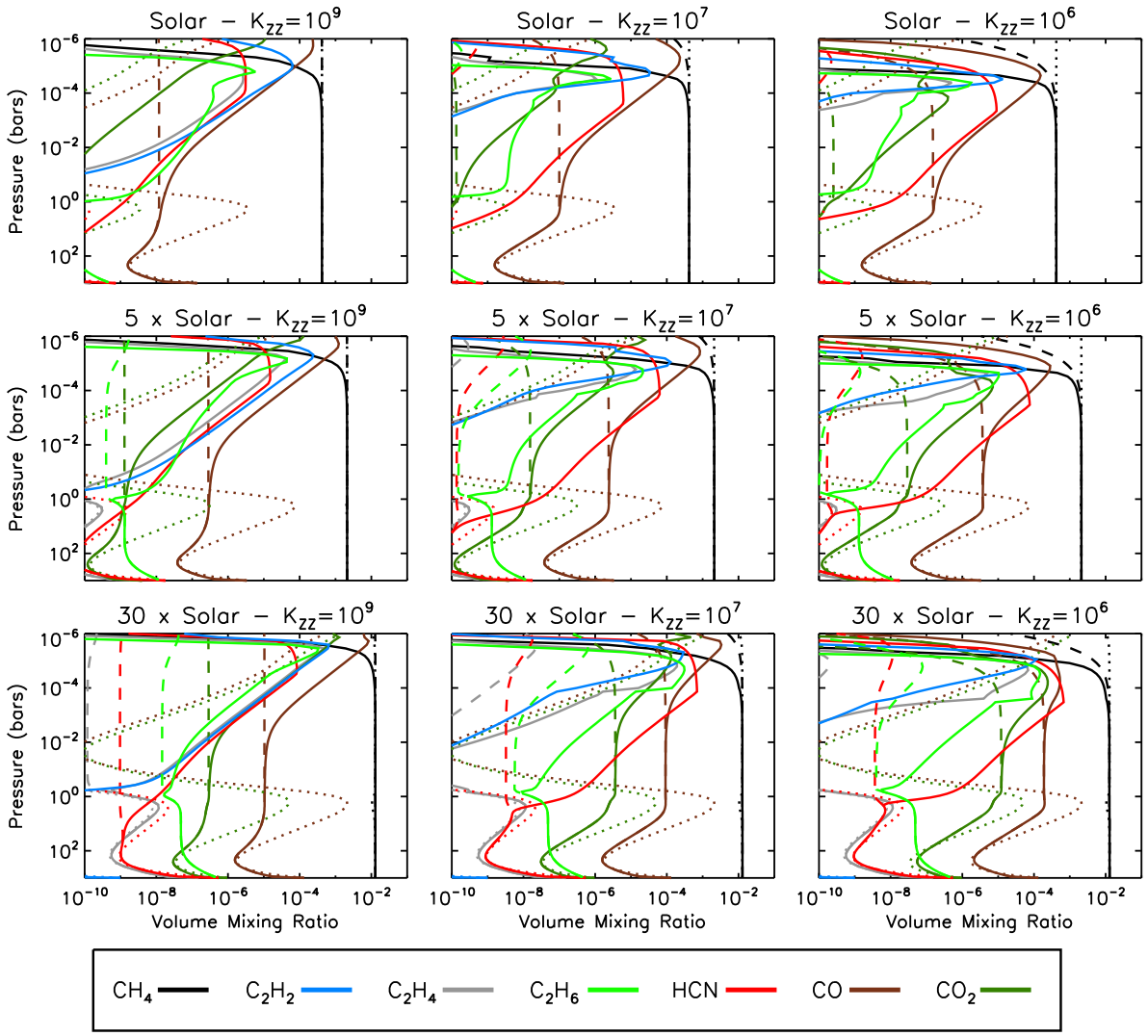


Fig. 3.— Same as Figure 2 but for the major carbon-bearing molecules only.

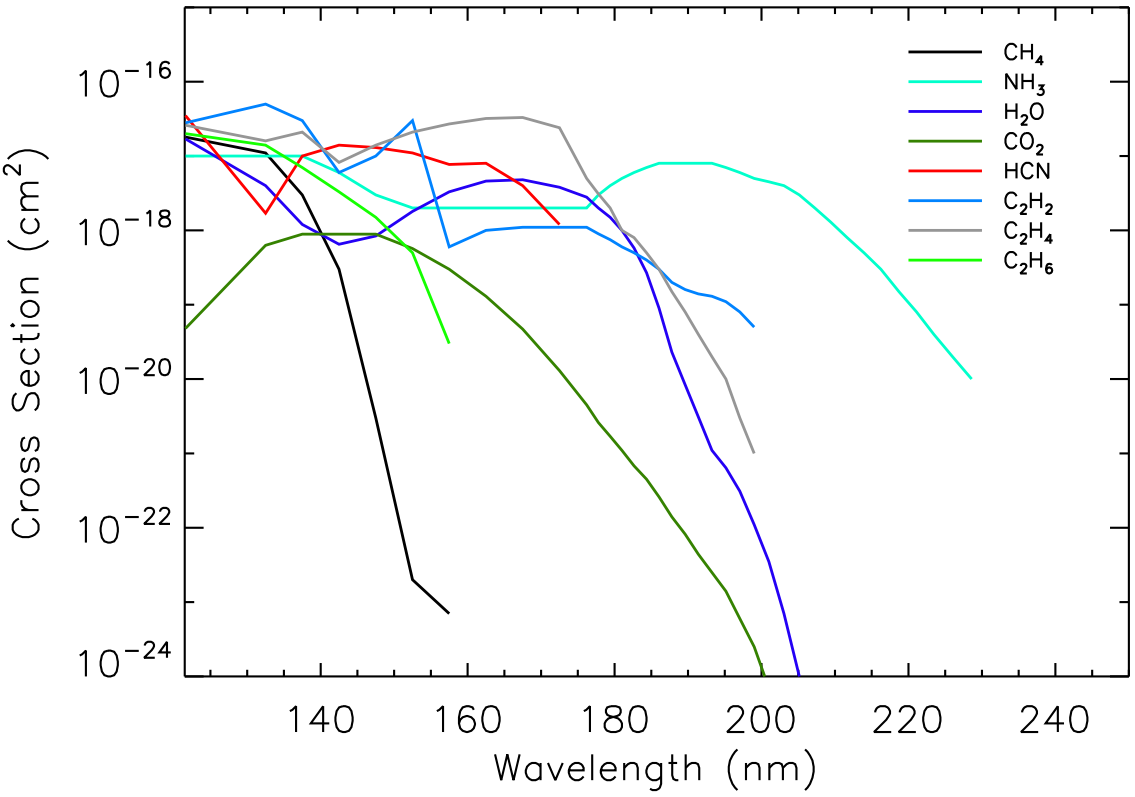


Fig. 4.— Photolysis cross sections for some of the molecules that are predicted to be present at high abundance in GJ 1214b's atmosphere. Photolysis rates are detemined by $\int \sigma F_\nu e^{-\tau_\nu} d\nu$ where $F_\nu$ is the stellar flux density, $\tau_\nu$ is the optical depth, and $\sigma$ is the photolysis cross section. The photolysis cross sections plotted here are from Zahnle et al. (2009a, and references therein).

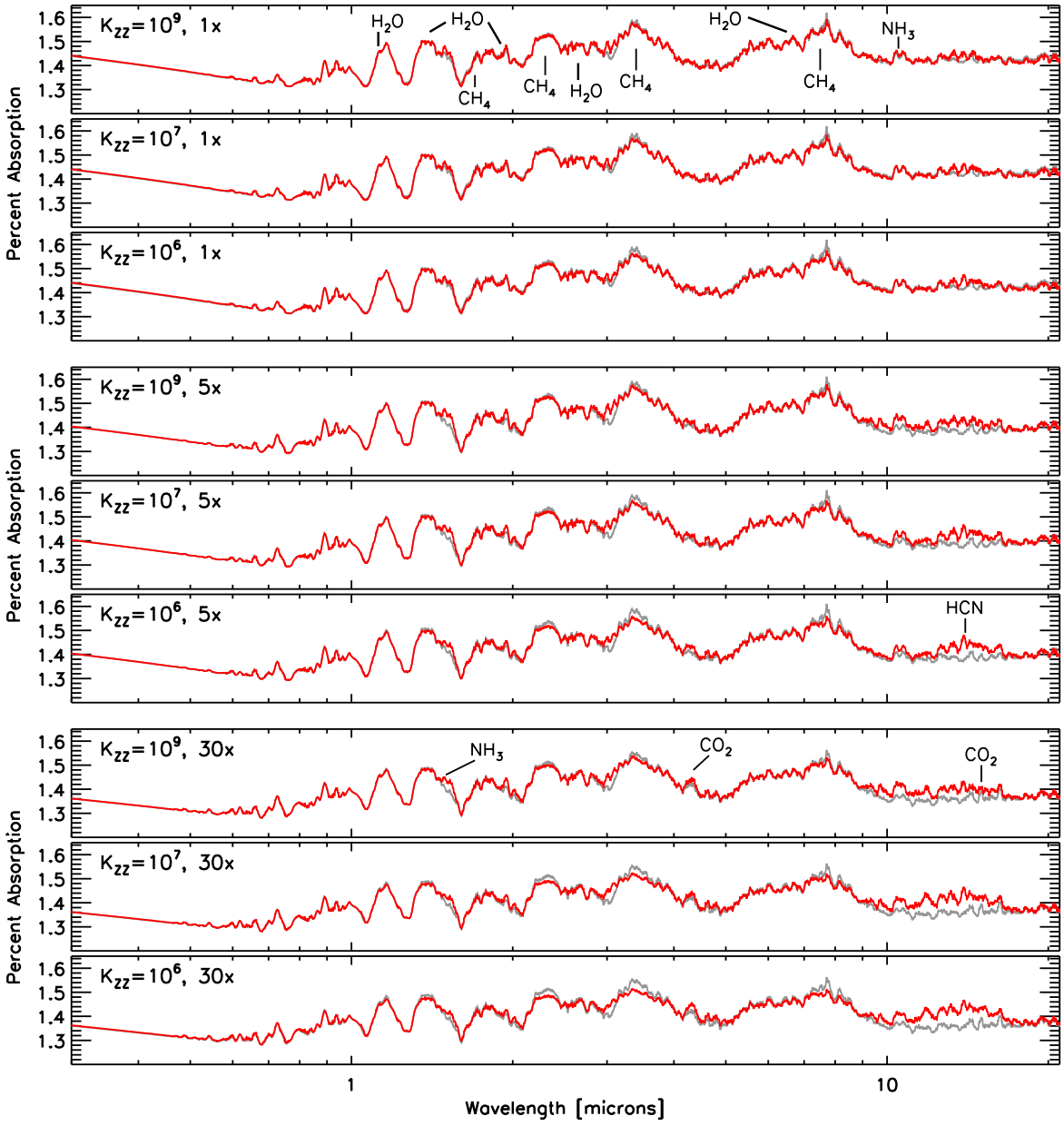


Fig. 5.— Transmission spectra for GJ 1214b given the atmospheric composition shown in Figures 2 and 3 for an active host star (AD Leo input spectrum) - red lines. For comparison, the spectra obtained for atmospheres in thermal equilibrium are shown in gray. For each panel, values for $K_{zz}$ and metallicity are indicated. Departures from the equilibrium spectra are mostly due to the re-budgeting of carbon away from methane into other molecules such as $CO_2$, and HCN. Major spectral features are as indicated. All spectra have been normalized so as to reproduce the observed transit depth of 1.35% in the MEarth bandpass.

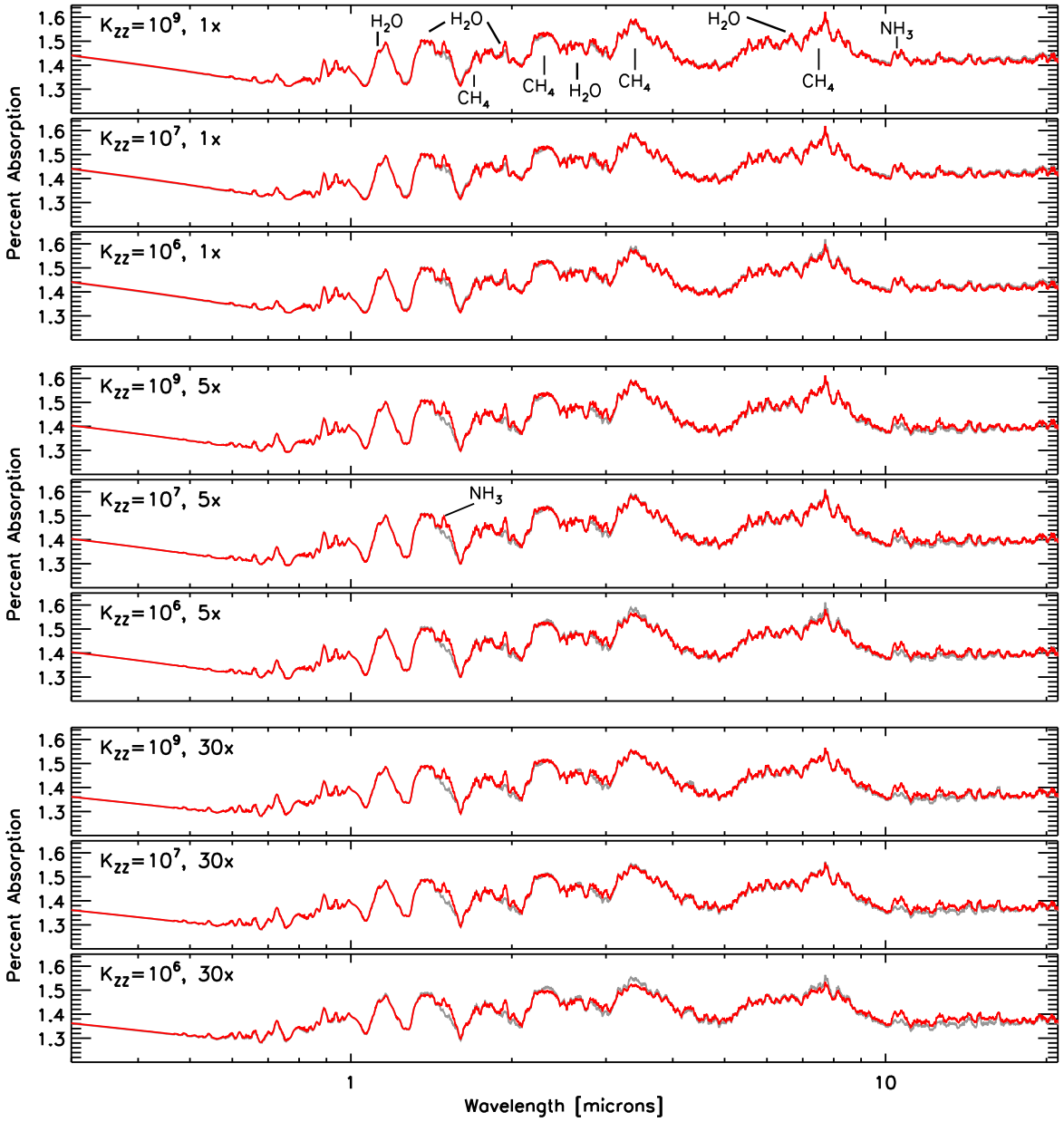


Fig. 6.— Same as Figure 5, but for a quiet host M-star. Here the non-equilibrium chemistry plays a lesser role in affecting the transmission spectrum, since methane remains stable to high elevations in the planet's atmosphere.

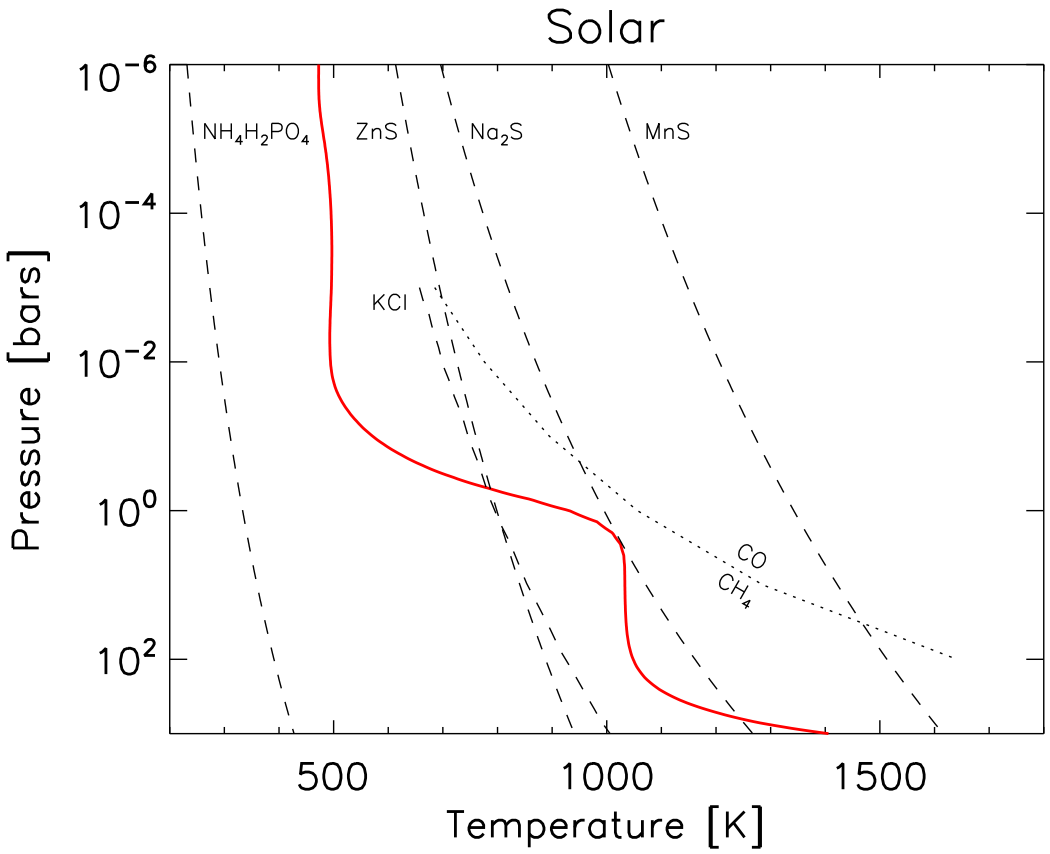


Fig. 7.— The calculated T-P profile for GJ 1214b at solar metallicity. Condensation curves for various molecules are overplotted as indicated. Species whose condensation curves cross the T-P profile will condense in GJ 1214b's atmosphere at the pressure indicated. KCl and ZnS are predicted to both condense at 500 mbar for solar composition. The CO/$CH_4$ equilibrium curve is also shown (dotted line), indicated that methane is predicted to be the dominant equilibrium carbon-bearing species throughout GJ 1214b's atmosphere. The CO-$CH_4$ curve shifts towards the left (to lower temperature) at higher metallicity and can even intersect the T-P profile at 30-50 times solar metallicity. However, this occurs above the quench point of CO/$CH_4$, so it has little effect on the atmospheric chemistry.

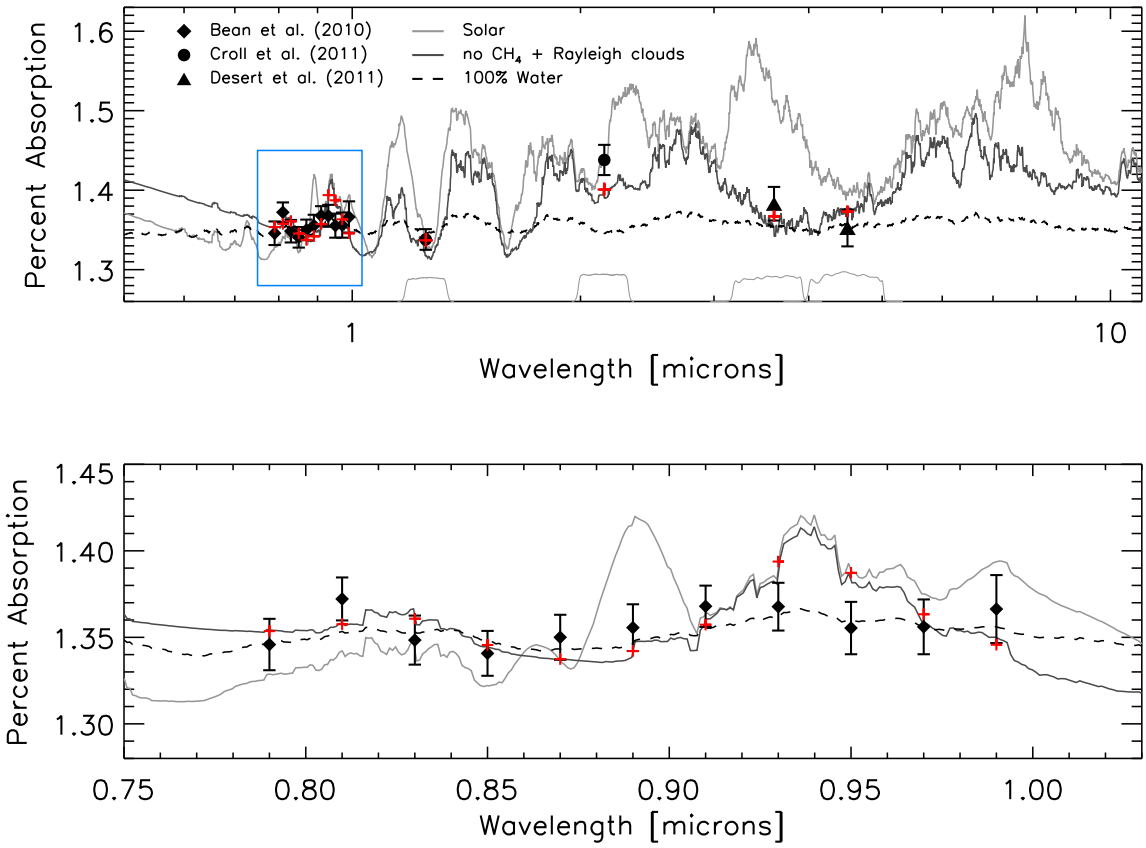


Fig. 8.— Comparisons of the transmission data for GJ 1214b from Bean et al. (2010), Désert et al. (2011), and Croll et al. (2011) to our model spectra (top). The same is shown for just the Bean et al. (2010) data in the bottom panel. The bandpasses for the Désert et al. (2011) and Croll et al. (2011) data are shown at the bottom of the upper panel for reference. The best fit to all of the data is obtained for a solar composition atmosphere with methane completely removed and clouds affecting the spectrum at short wavelengths (dark gray solid curve). Clouds have been simulated here by increasing the nominal Rayleigh scattering opacity by a factor of 5. Red "+" signs show the expected values of the transit depth based on the best-fit model, averaged over the bandpasses of each observed data point. The transmission spectrum for a 100% water steam atmosphere provides the second-best fit to the data (dashed black curve) but is in strong disagreement with the Croll et al. (2011) Ks-band data point. The transmission spectrum for a solar composition atmosphere in chemical equilibrium is overplotted for reference (solid light gray curve).